Brain Pathology ISSN 1015-6305

RESEARCH ARTICLE

BRAF-Mutated Pleomorphic Xanthoastrocytoma is Associated with Temporal Location, Reticulin Fiber Deposition and CD34 Expression

Christian Koelsche[1,2]; Felix Sahm[1,2]; Adelheid Wöhrer[3]; Astrid Jeibmann[4]; Jens Schittenhelm[5]; Patricia Kohlhof[6]; Matthias Preusser[7,8]; Bernd Romeike[9]; Hildegard Dohmen-Scheufler[10]; Christian Hartmann[11]; Michel Mittelbronn[12,13,14]; Albert Becker[15]; Andreas von Deimling[1,2]; David Capper[1,2]

[1] Department of Neuropathology, Ruprecht-Karls-Universität Heidelberg, Heidelberg, Germany.
[2] German Cancer Consortium (DKTK), CCU Neuropathology, German Cancer Research Center (DKFZ), Heidelberg, Germany.
[3] Institute of Neurology, Medical University of Vienna, Vienna, Austria.
[4] Institute of Neuropathology, University Hospital Münster, Münster, Germany.
[5] Department of Neuropathology, Institute for Pathology and Neuropathology, University of Tübingen, Tübingen, Germany.
[6] Department of Pathology, Klinikum Stuttgart, Katharinenhospital, Stuttgart, Germany.
[7] Comprehensive Cancer Center, Medical University of Vienna, Vienna, Austria.
[8] Department of Medicine I, Medical University of Vienna, Vienna, Austria.
[9] Institute of Pathology, Department of Neuropathology, Jena University Hospital, Friedrich Schiller University, Jena, Germany.
[10] Institute of Neuropathology, Medical School, Justus Liebig University, Giessen, Germany.
[11] Department for Neuropathology, Hannover Medical School, Hanover, Germany.
[12] Neurological Institute (Edinger-Institut), Goethe University, Frankfurt am Main, Germany.
[13] German Cancer Consortium (DKTK), Heidelberg, Germany.
[14] German Cancer Research Center (DKFZ), Heidelberg, Germany.
[15] Department of Neuropathology, University of Bonn, Bonn, Germany.

Keywords
brain tumor, *BRAF* V600E, *CDKN2A*, CD34, immunohistochemistry, pleomorphic xanthoastrocytoma, p16, VE1.

Corresponding author:
David Capper, MD, Department of Neuropathology, Ruprecht-Karls-Universität Heidelberg, Im Neuenheimer Feld 224, D-69120 Heidelberg, Germany (E-mail: *david.capper@med.uni-heidelberg.de*)

Received 10 September 2013
Accepted 20 November 2013
Published Online Article Accepted 18 December 2013

Conflict of interest: David Capper and Andreas von Deimling have applied for a patent on the diagnostic use of *BRAF* V600E mutant-specific antibody VE1. All terms are being managed by the German Cancer Research Center in accordance with its conflict of interest policies. The other authors do not have any conflicts of interest to disclose.

doi:10.1111/bpa.12111

Abstract

BRAF V600E mutation and homozygous deletion of *CDKN2A* (p16) are frequent molecular alterations in pleomorphic xanthoastrocytomas (PXAs). We investigated 49 PXAs for clinical, histological and immunohistochemical characteristics related to *BRAF* mutation status. *BRAF* mutation was detected by immunohistochemical assay and DNA sequencing in 38/49 (78%) tumors. All but one PXA located in the temporal lobe harbored a *BRAF* V600E mutation (23/24; 96%) compared with 10/19 nontemporal PXAs (53%; $P = 0.0009$). Histological and immunohistochemical analysis demonstrated increased reticulin deposition (76% vs. 27%; $P = 0.003$) and a more frequent expression of CD34 in *BRAF*-mutant PXAs (76% vs. 27%; $P = 0.003$).

We further investigated the utility of combined *BRAF* V600E (VE1) and p16 analysis by immunohistochemistry to distinguish PXAs from relevant histological mimics like giant-cell glioblastoma. Among PXAs, 38/49 (78%) were VE1-positive, and 30/49 (61%) had a loss of p16 expression. The combined features (VE1 positivity/p16 loss) were observed in 25/49 PXAs (51%) but were not observed in giant-cell glioblastoma (VE1 0/28, p16 loss 14/28). We demonstrate that temporal location, reticulin deposition and CD34 expression are associated with *BRAF* mutation in PXA. Combined VE1 positivity and p16 loss represents a frequent immunoprofile of PXA and may therefore constitute an additional diagnostic tool for its differential diagnosis.

INTRODUCTION

Pleomorphic xanthoastrocytoma (PXA) is a rare glial tumor mostly affecting children and adolescents. The tumor is often localized in superficial regions of the neocortex and typically presents with a well-circumscribed growth (15). The histological appearance of PXA is characterized by the presence of pleomorphic giant tumor cells with bizarre shape, foamy/xanthomatous cytoplasm, multinucleation and nuclear atypia in absence of mitotic activity (16, 17). Furthermore, a dense reticulin network frequently surrounds these tumor cells (15). The predominant expression of glial fibrillary acidic protein (GFAP) indicates a mostly astrocytic differentiation, but expression of neuronal markers has also been detected in a considerable fraction of PXAs (17). Therefore, a sharp demarcation between PXA and glioneuronal tumors, especially ganglioglioma, may be challenging in some instances.

Despite their pleomorphic appearance, PXAs often have a more favorable clinical outcome compared with high-grade astrocytomas with similar histological features (27). Such cases correspond to WHO grade II and are designated as PXA II in this article (15). Nevertheless, malignant histological features have been observed in up to 20% of PXA cases (16, 18, 26, 35). Such cases, designated as PXA with anaplastic features (PXA-AF), are prone to recurrence and have a less favorable prognosis (16).

The molecular biology of PXA is currently under investigation. Recently, v-Raf murine sarcoma viral oncogene homolog B1 (*BRAF*) mutations have been detected in up to 70% of PXAs (12, 13, 33, 34) and have become recognized as a hallmark genetic alteration in these tumors. In two recent exome and extensive panel sequencing studies of a total of 20 PXAs, cases without *BRAF* mutations (n = 7) either had no detectable mutations (n = 4) or harbored mutations of *TSC2* (n = 1) or *NF1* (n = 1) or an *ETV6–NTRK3* fusion (n = 1) (2, 40). Further, several case reports have previously pointed out a possible association of *NF1* germ-line mutation carriers with the development of PXA (1). Another frequent alteration in PXA is the loss of chromosome locus 9p21, resulting in homozygous deletion of *CDKN2A* (coding for p16) in up to 60% of cases (39).

A second predominantly pediatric brain tumor with frequent *BRAF* V600E mutations is ganglioglioma. In a previous project we sought to further characterize ganglioglioma in relation to *BRAF* mutation status and were able to demonstrate strong associations of *BRAF* mutation status with expression of synaptophysin, presence of dysplastic neurons, presence of lymphocytic cuffs and younger patient age (24). An immunohistochemical assay using *BRAF* V600E mutation-specific antibody VE1 further demonstrated that dysplastic neurons were frequent target cells of *BRAF* mutation (10, 24).

In PXA, detection of *BRAF* V600E-mutated protein by VE1 immunohistochemistry has recently been investigated by two independent studies, both demonstrating high sensitivity and specificity (8, 19).

Although *CDKN2A* deletions are frequent in PXA, loss of p16 protein expression in PXA has so far not been further investigated. For glioblastoma, an immunohistochemical approach for assessing p16 status had a high sensitivity (81.5%) for combined homozygous and hemizygous deletions (sensitivity for homozygous alone was 95%), although specificity was not optimal (70%), with 30% of cases without *CDKN2A* deletions showing negative p16 immunohistochemistry (29).

Here we investigated a large series of 49 PXAs for clinical, histological and immunohistochemical characteristics in relation to *BRAF* mutation status. Further, we investigated the utility of combined VE1 and p16 immunohistochemistry to separate PXA from the clinically relevant differential diagnoses ganglioglioma and giant-cell glioblastoma.

MATERIALS AND METHODS

Tissue samples, patient characteristics and histology

In total, 49 PXAs (32 PXA II and 17 PXA-AF; Supporting Information Table S1) were included in this study. Tissue samples were retrieved from the archives of the Department of Neuropathology of Ruprecht-Karls-Universität Heidelberg, the Department of Neuropathology of the University of Hannover, the Institute for Neuropathology of the University of Münster, the Department of Neuropathology of the University of Jena, the Institute of Neuropathology of Justus Liebig University Giessen, the Department of Pathology of the Klinikum Stuttgart, the Institute for Pathology and Neuropathology of the University of Tübingen, the Department of Neuropathology of the University of Bonn, the Institute of Neurology of the Medical University of Vienna and the Institute of Neurology (Edinger-Institut) of Goethe University in Frankfurt. All tumors were reviewed by members of the Department of Neuropathology at Heidelberg (CK, FS, AvD, DC) and diagnosed according to the revised WHO 2007 classification of brain tumors. Additional patient characteristics are given in Supporting Information Table S1. Hematoxylin-and-eosin (HE)- and reticulin-stained slides of all cases were evaluated for the presence of dysplasia in neurons, multinucleated cells, giant cells, xanthomatous cells, perivascular cuffs of lymphocytes, eosinophilic granular bodies, nuclear inclusions, Rosenthal fibers, angiocentric growth pattern, calcifications and extensive hemosiderin deposition. Further assessment was made of structure of tumor matrix, proliferation (mitoses per 10 high-power fields, HPFs), microvascular proliferation, prominence of capillary network and extent of argyrophilic fibers. These parameters were assessed in 10 suitable HPFs. Intercellular reticulin deposition (argyrophilic fibers) was scored as absent if confined to vessel walls. Furthermore, 28 giant-cell glioblastomas were analyzed for VE1, p16 and CD34 immunohistochemistry and extent of argyrophilic fibers (Supporting Information Table S2).

Immunohistochemistry

Prior to additional investigations, all cases were tested to ensure they were negative for *IDH1* R132H mutation, either by immunohistochemistry (clone H09) or by *IDH1* Sanger sequencing as previously described (6). Sections cut to 4 μm were dried at 80°C for 15 minutes and stained with *BRAF* V600E-specific clone VE1 on a Ventana BenchMark XT immunostainer (Ventana Medical Systems, Tucson, AZ, USA). The Ventana staining procedure included pretreatment with cell conditioner 1 (pH 8) for 64 minutes, followed by incubation with VE1 hybridoma supernatant (monoclonal, dilution 1:5) at 37°C for 32 minutes. Antibody

incubation was followed by incubation with OptiView HQ Universal Linker (Ventana) for 12 minutes, incubation with OptiView HRP Multimer (Ventana) for 12 minutes, signal amplification using the Ventana OptiView Amplification Kit (Ventana, catalogue number 760-099), and counterstaining with one drop of hematoxylin for 4 minutes and one drop of bluing reagent for 4 minutes. As positive and negative controls, a tissue microarray consisting of four melanoma samples of known *BRAF* V600 status (two wild-type, two *BRAF* V600E) was included in every staining run.

Immunohistochemistry was also performed with antibodies for detecting GFAP (polyclonal, code Z0334, 1:1000, Dako, Glostrup, Denmark), CD34 (clone QBEnd10, 1:2, Thermo Scientific, Waltham, MA, USA), synaptophysin (clone SY38, 1:20, Dako), Ki-67 (clone SP6, 1:100, Cell Marque Corporation, Rocklin, CA, USA) and phosphorylated extracellular signal-regulated kinase (pERK; polyclonal, 1:200, Cell Signaling, Danvers, MA, USA); polyclonal, 1:200, Cell Signaling, Danvers, MA, USA) using standard staining procedures, employing the UltraView Universal DAB Detection Kit (Ventana). Anti-p16 antibody (clone G175–405, 1:200, Becton Dickinson Biosciences, Franklin Lakes, NJ, USA) was visualized with the Ventana OptiView kit under standard conditions.

For evaluation of pERK and p16, tumors with at least 5% of tumor cell nuclei stained were scored positive. Staining of vessels or clearly reactive glia was not considered. VE1 and IDH1 were scored as either positive or negative. For both antibodies, nonspecific staining of macrophages, eosinophilic granular bodies and calcified deposits was observed and was not considered for scoring. For Ki-67 analysis, tumor areas with the highest Ki-67 labeling index were evaluated for the fraction of positive cells by counting all cells, excluding vascular cells and lymphocytes, in one 200× microscopic field using a counting grid. The semiquantitative immunoreactive score (IRS) for synaptophysin, GFAP and CD34 (31) was calculated as previously described (24). Photographs were taken with a BX53 microscope (Olympus, Tokyo, Japan) equipped with an SC30 digital color camera (Olympus) and Olympus cellSens software.

Sequencing and statistics

BRAF sequencing results of parts of this series were previously reported by Schindler *et al* (34). For the remaining cases, PCR amplification and sequencing for codon 600 of *BRAF* were performed as described (34). For DNA extraction, areas of the tumor with the highest available DNA content were chosen and macrodissected. For VE1-positive cases, areas with the highest concentration of VE1-positive tumor cells were selected for DNA extraction. In one PXA, Sanger sequencing failed to confirm a *BRAF* V600E mutation detected by immunohistochemistry, but its presence was confirmed by additional pyrosequencing. Pyrosequencing was performed as previously described (23). All sequencing reactions were carried out in forward and reverse directions. Mutations were identified by visual analysis of the sequence chromatograms using Sequence Pilot software, version 3.1 (JSI-Medisys, Kippenheim, Germany). GenBank sequence NM_004333 for *BRAF* (National Center for Biotechnology Information, Bethesda, MD, USA) was used as reference.

A χ^2-test (Pearson) was used to examine associations between nominal variables. Student's *t*-test was used to examine the association between nominal and continuous variables. Significance was defined as $P < 0.05$. JMP 9.0 was used for statistical analysis.

RESULTS

VE1 immunohistochemistry and *BRAF* mutations in PXA

Mutated BRAF V600E protein was detected in 38/49 (78%) of PXAs. The vast majority of PXA tumor cells were stained by the VE1 immunohistochemical assay, irrespective of their highly variant shapes (Figures 1A and 2A). However, immunohistochemical staining was frequently more intense in the ballooned and xanthomatous cell types (Supporting Information Figure S1). DNA sequencing (Sanger sequencing and, in one case, pyrosequencing) could be performed in 45 cases and confirmed the immunohistochemically detected presence or absence of the *BRAF* V600E mutation in all cases (Supporting Information Table S1). Sequencing revealed a single PXA with a *BRAF* 599insT mutation not detected by VE1. In one case with low tumor burden, the *BRA*F mutation could only be confirmed by pyrosequencing (data not shown).

No differences in the *BRAF* mutation rates were observed between PXA II (26/33; 79%) and PXA-AF (12/16; 75%).

Clinical, immunohistochemical and histological features of PXA in relation to *BRAF* status

The available clinical data for this study comprised tumor location, patient age at operation and gender. Tumor location was available in 43 cases, with 24 tumors originating in the temporal lobe and 19 in other parts of the brain (Table 1). Analysis of *BRAF* mutation status revealed that 23/24 (96%) of temporally located tumors were *BRAF* V600E-mutated, whereas in other locations only 10/19 (53%) harbored this genetic alteration ($P = 0.0009$). The association of *BRAF* mutation with location was significant for both PXA II ($P = 0.004$) and PXA-AF ($P = 0.05$). Patients with *BRAF*-mutated PXA were younger at operation, but this did not reach statistical significance ($P = 0.06$; Table 1). No associations between gender and *BRAF* status were observed (Table 1).

Immunohistochemical analysis of the series was carried out for synaptophysin, GFAP, CD34, pERK, p16 and Ki-67 (Table 1). Of these, only CD34 was differentially expressed between *BRAF* wild-type and *BRAF* mutant PXA. CD34 expression was present in 29/38 PXAs (76%) with the *BRAF* V600E mutation and only 3/11 PXAs (27%) without it ($P = 0.003$) (Figure 1A,B). CD34 expression was more frequently detected in PXA II (70%) than in PXA-AF (56%). The staining pattern of most CD34-positive tumor cells was either cytoplasmic (Figure 2C) or a more pericellular, stroma-like binding (Figure 1A). Adjacent to solid tumor areas we frequently observed isolated CD34-positive cells, sometimes with the previously described "bushy" staining (11) or reminiscent of "satellite" cells (3) (Figure 2D). On serial sectioning, these isolated CD34-positive cells were often also found to be VE1-positive (Figure 2). Results of the other immunohistochemical staining assays are summarized in Table 1.

Among the diverse histological features investigated in PXA (Table 1), only the presence of reticulin fibers was significantly associated with *BRAF* mutation (Figure 1). This feature was

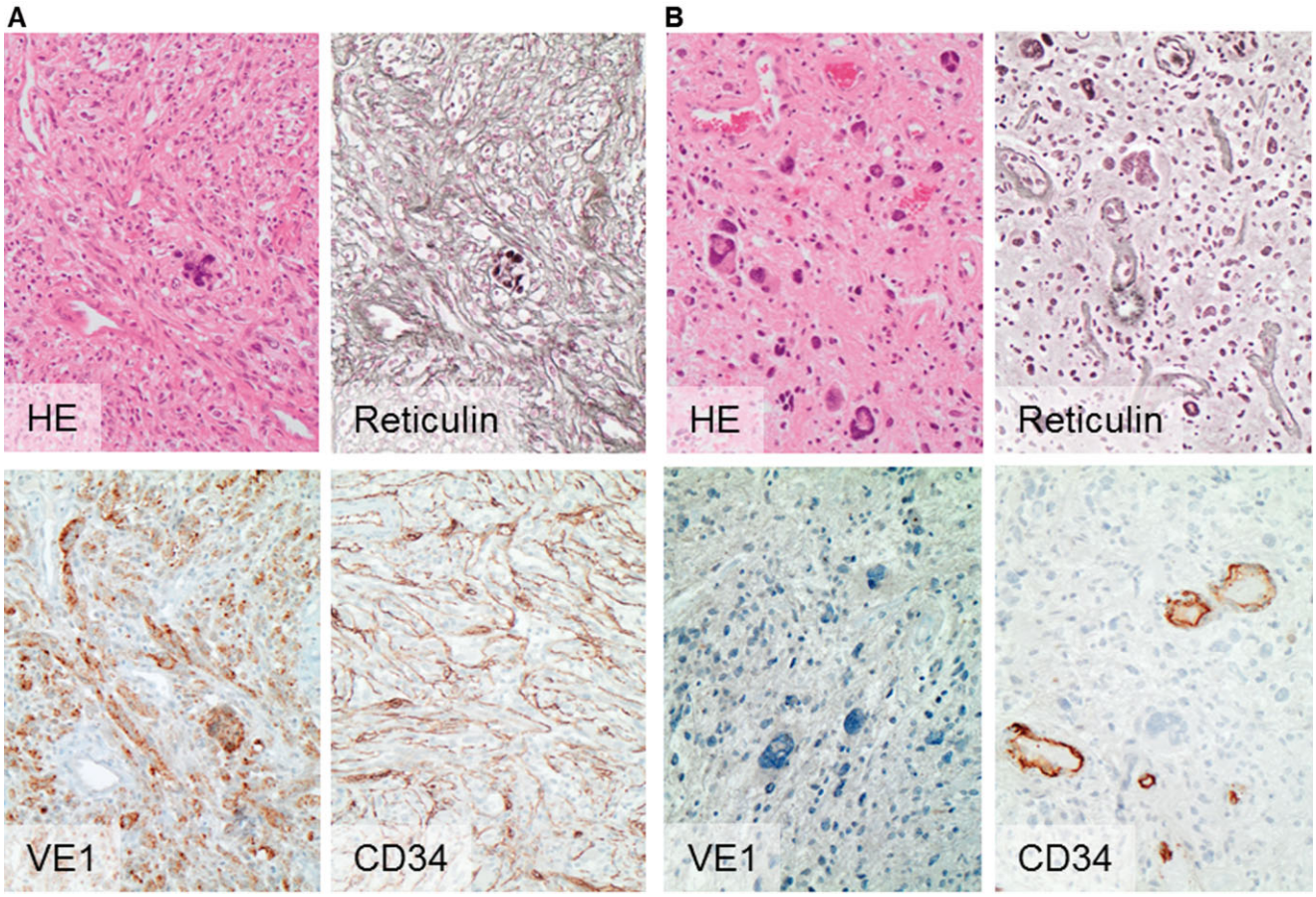

Figure 1. *Histology and immunohistochemistry of PXA in relation to BRAF status.* PXA (id 60350) of temporal location with *BRAF* V600E mutation (**A**) compared with a PXA (id 61998) of nontemporal location of *BRAF* wild-type status and without VE1 binding (**B**). Note the abundance of pericellular reticulin fiber deposits in and the CD34 expression of tumor cells in **A**, whereas PXAs of *BRAF* wild-type status are more likely to be associated with absence of pericellular reticulin deposits and restriction of CD34 expression to the vasculature, as exemplified in case **B**. Magnification: 200×. HE, hematoxylin and eosin.

present in 29/38 *BRAF*-mutated cases (76%) but in only 3/11 (27%) without *BRAF* mutation. Additional investigated histological parameters and results are compiled in Table 1; unprocessed data can be reviewed in Supporting Information Table S1.

Combined analysis of *BRAF* VE1 and p16 expression for PXA differential diagnosis

PXAs are characterized by a high frequency of *BRAF* V600E mutation and deletions of *CDKN2A* (p16). As both features can readily be assessed by immunohistochemistry, we further investigated the utility of combined VE1 and p16 analysis to separate PXA from the clinically relevant differential diagnoses giant-cell glioblastoma and ganglioglioma (Table 2). For p16 analysis, we employed an antibody that has previously demonstrated high specificity (14).

In PXA, p16 loss was observed in 30/49 tumors (61%). As noted above, VE1 was positive in 38/49 cases (78%). No statistical association between VE1 and p16 was observed in PXA ($P = 0.22$). The combined features of VE1 positivity and p16 loss were observed in 25/49 PXAs (51%) (Table 2). We additionally analyzed 28 cases of giant-cell glioblastoma and observed no case positive for VE1, whereas 14/28 cases showed a loss of p16 (Table 2). None of the cases presented with the combined features of VE1 positivity and p16 loss (Table 2, Supporting Information Table S2).

We previously investigated a large cohort of ganglioglioma for both VE1 and p16 immunohistochemistry (24). In that study, VE1 positivity was frequent (41/71; 58%), whereas p16 loss was only observed in 6/63 (10%) gangliogliomas, and only 3/63 (5%) cases showed combined VE1 positivity and p16 loss (Table 2; Supporting Information Table S3). Typical staining patterns for VE1 and p16 of PXA, giant-cell glioblastoma and ganglioglioma are compiled in Figure 3.

DISCUSSION

Our investigation confirms exceedingly high *BRAF* V600E mutation rates in PXA. The incidence of *BRAF* V600E mutation in this series is slightly higher than in previous reports relying on

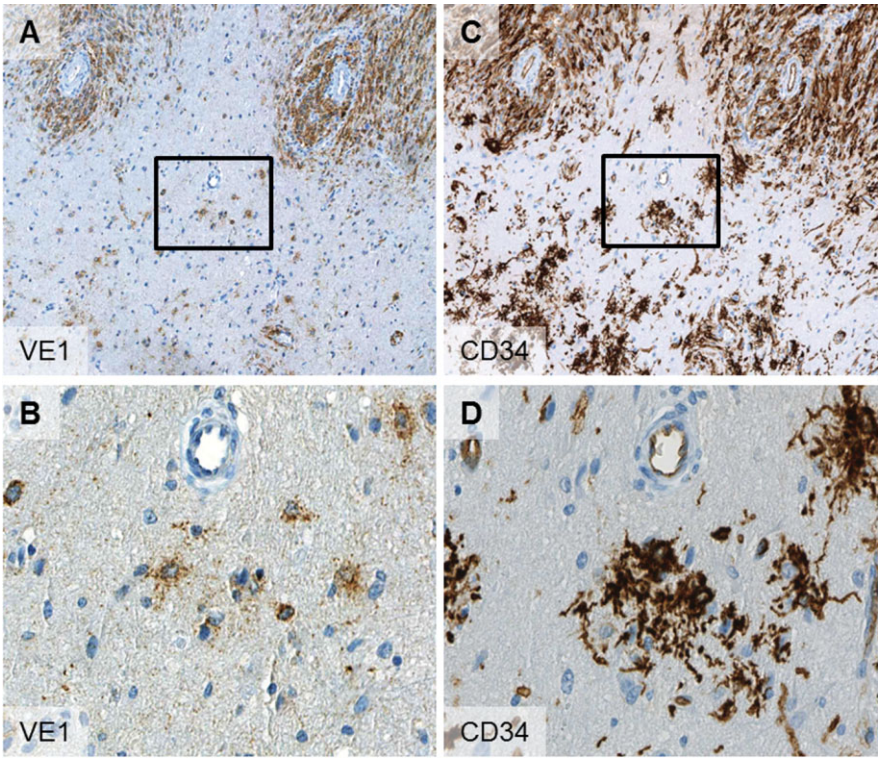

Figure 2. *Serial sections of border zone of PXA (id 60358)* with solid tumor areas (**A**,**C** upper areas) and infiltration zone (**A**,**C** lower areas). Note the high congruence of VE1 and CD34 expression in the solid tumor areas as well as in adjacent "satellite" cells in the infiltration zone (**B**,**D**). The boxes in (**A**) and (**B**) indicate the field of higher magnification seen in (**B**) and (**D**). Magnification: 100× (**A,C**); 400× (**B,D**).

DNA-based methods for mutation detection (12, 13, 34). This is most likely a result of the capability of VE1 immunohistochemistry to detect the mutation in tissues with a low tumor burden and of the rigorous macrodissection approach we applied in obtaining DNA for sequence confirmation. As *BRAF* V600E-targeted therapy may in future become an additional therapeutic option for recurrent PXA or PXA undergoing malignant progression (7), implementation of such stringent assays for diagnostic detection of *BRAF* mutations may soon become essential.

On the other hand, one case with a rare *BRAF* 599insT mutation was not detected by VE1 immunohistochemistry. Thus, our findings confirm previous observations in other tumor entities that VE1 immunohistochemistry is of a slightly higher sensitivity compared with Sanger sequencing but may fail to detect the rarer types of *BRAF* mutations (5, 9, 23–25, 36). However, in contrast to melanoma, with its considerable frequencies of *BRAF* V600K and other *BRAF* mutations, alterations other than *BRAF* V600E seem to be exceedingly rare in PXA.

BRAF mutation rates were surprisingly close for PXA II (79%) and PXA-AF (75%). This demonstrates the expected close relationship between PXA II and PXA-AF; on the other hand, this indicates that *BRAF* V600E mutation is likely an early event in the tumorigenesis of PXA and is likely not a driver of malignant progression to PXA-AF.

Our analysis of associations between *BRAF* mutation status and clinicopathological characteristics revealed temporal location as the most significant factor. Our series indicates that temporally located PXAs almost certainly harbor *BRAF* mutations and adds to the growing body of evidence for specific relationships between genotype and location of brain tumors, as recently demonstrated for mutations of *H3F3A* (37). Interestingly, such a relationship between location and *BRAF* status was not observed in our previous series of gangliogliomas, which otherwise showed a similar predilection for the temporal lobe (24). This indicates that such associations between mutation and location may be tumor type-specific.

In the same study we observed a significant association between younger age and *BRAF* mutation for ganglioglioma (24). While patients with *BRAF*-mutated PXA were also younger (median 21 vs. 27 years) the difference did not reach statistical significance ($P = 0.06$).

A prominent network of reticulin fibers has been recognized as a hallmark histological feature of PXA (20). Here we demonstrate that the presence of reticulin fibers is strongly associated with the presence of *BRAF* mutations. An association of *BRAF* mutation with a more mesenchymal differentiation and prominent intercellular reticulin deposition was also observed in a smaller series of PXAs by Dias-Santagata *et al* (12), further corroborating our observation. It is not clear whether *BRAF* plays a functional role in this mesenchymal shift. In our previous series of gangliogliomas, reticulin fiber deposition was not associated with *BRAF* mutation—a result not supporting, if not ruling out, a functional connection (24). Interestingly, in thyroid cancer a link between *BRAF* mutation and epithelial–mesenchymal transition has been established. In a mouse model of thyroid cancer, overexpression of *BRAF* V600E renders thyroid cells susceptible to transforming growth factor β (TGF-β)-induced epithelial–mesenchymal transition (22). In a different model of thyroid cancer, *BRAF* V600E even directly induced TGF-β secretion (32). It would be interesting

Parameter	*BRAF* V600E	*BRAF* wild type	*P* value
Patient age (years), median (range) (n = 49)	21 (5–74)	27 (18–65)	0.06
Patient sex (male, female) (n = 49)	20, 18	8, 3	0.326
Tumor location (temporal, other) (n = 43)	23, 10	1, 9	0.0009
Growth pattern (fibrillary, other) (n = 48)	24, 13	6, 5	0.54
Immunohistochemical characteristics			
Synaptophysin-positive (n = 49), n (%)	8/38 (21)	2/11 (18)	0.84
GFAP-positive (n = 49), n (%)	34/38 (94)	11/11 (100)	0.26
CD34-positive (n = 49), n (%)	29/38 (76)	3/11 (27)	0.003
pERK-positive (n = 49), n (%)	24/38 (63)	9/11 (82)	0.25
p16 loss (n = 49), n (%)	25/38 (66)	5/11 (45)	0.22
Ki-67-positive (%), mean (95% CI) (n = 48)	5.0 (2.9–7.0)	6.1 (2.3–9.9)	0.6
Histological characteristics, n (%)			
Eosinophilic granular bodies	33/38 (87)	8/11 (73)	0.26
Reticulin fibers	29/38 (76)	3/11 (27)	0.003
Lymphocytic cuffs	10/38 (26)	4/11 (36)	0.52
Xanthomatous tumor cells	22/38 (58)	7/11 (63)	0.73
Dysplastic neurons	3/38 (8)	0/11 (0)	0.34
Pleomorphic/multinucleated cells	32/38 (84)	11/11 (100)	0.16
Giant cells	13/36 (36)	3/9 (33)	0.88
Rosenthal fibers	11/38 (29)	2/11 (18)	0.48
Tumoral calcifications	7/38 (18)	1/11 (9)	0.46
Extensive hemosiderin deposition	3/38 (8)	0/11 (0)	0.34
Nuclear inclusions	30/38 (79)	8/11 (72)	0.66
Angiocentric growth	4/38 (11)	2/11 (18)	0.5
Prominent capillary network	0/38 (0)	0/11 (0)	1
Endothelial proliferation	12/38 (32)	4/11 (36)	0.77
Necrosis	9/38 (24)	3/11 (27)	0.81
Mitoses (at least 1 in 10 high-power fields)	15/38 (39)	5/11 (45)	0.72

Table 1. Correlation of *BRAF* V600E status with clinical data, histology and immunohistochemical features in pleomorphic xanthoastrocytomas.

to investigate if mutated *BRAF* also has a functional interaction with TGF-β-mediated signaling in brain tumors.

CD34 is a typical diagnostic marker for PXA and was found in up to 73% of cases in a series by Reifenberger *et al* (30). This was confirmed in the present series (32/49 PXA, 65%); in line with previous reports, CD34 expression was more frequently detected in PXA II (70%) than in PXA-AF (56%). CD34 was the only immunohistochemical marker in our series showing significant associations with *BRAF* mutation. The cause of this association is not clear, but a recent study by Prabowo *et al* demonstrated associations between *BRAF* V600E and CD34 expression in both ganglioglioma and dysembryoplastic neuroepithelial tumors (28), indicating that our observation does not apply only to PXA. The CD34 staining pattern was concordant with patterns observed in epilepsy-associated tumors (3, 8, 11, 38), and samples with infiltration zone and adjacent cortex available for investigation repeatedly presented with the previously described "bushy" CD34 staining in adjacent tissue and more distant CD34-positive "satellite" cells (3). The nature of these "satellite" cells is unclear, but they have been considered as dysplastic and/or neoplastic transformed precursor cells (4). In our observations, CD34-positive "satellite-like" cells in PXA frequently coexpressed *BRAF* V600E-mutated protein (Figure 2), thus identifying this cell population as an integral part of the transformed cell population in PXA.

Table 2. VE1 and p16 immunohistochemistry in pleomorphic xanthoastrocytomas, giant-cell glioblastomas and gangliogliomas.

	Pleomorphic xanthoastrocytoma (n = 49)	Giant-cell glioblastoma (n = 28)	Ganglioglioma (n = 71)*
VE1 positivity, *n* (%)	38/49 (78)	0/28 (0)	41/71 (58)
Loss of p16 expression, *n* (%)	30/49 (61)	14/28 (50)	6/63 (10)
Both (%)	51	0	5

The combination of *BRAF* V600E mutation and loss of p16 expression is encountered in half of pleomorphic xanthoastrocytomas but is rarely observed in gangliogliomas and absent in giant-cell glioblastomas.
*Koelsche *et al* (24).

Diagnostic differentiation of PXA and other primary brain tumors, especially ganglioglioma and giant-cell glioblastoma, may be challenging. We therefore investigated the application of combined VE1 and p16 immunohistochemistry for this diagnostic question.

We observed p16 loss in 61% of PXAs, which is well in line with the expected 50–60% rate of homozygous *CDKN2A* deletions in these tumors (39). The combined features of VE1 positivity and p16 loss were observed in 51% of PXAs. All giant-cell glioblastomas were VE1-negative, confirming our previous genetic investigation of 15 giant-cell glioblastomas where we did also not detect *BRAF* mutations (34). The combined features (VE1

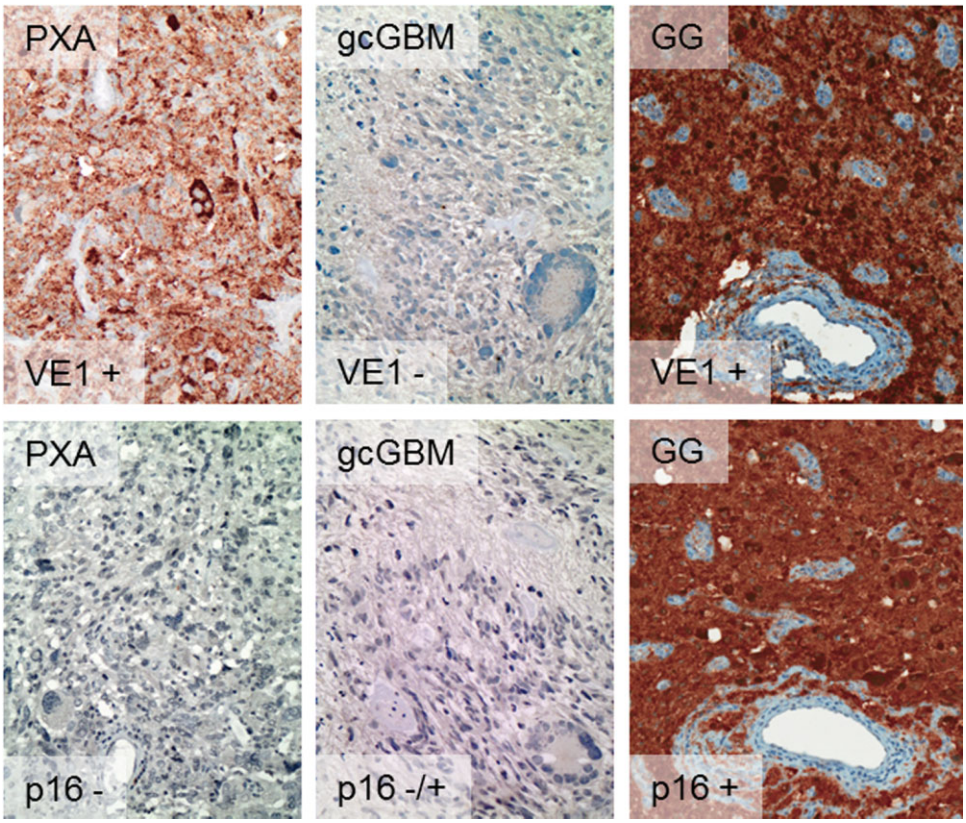

Figure 3. *Typical VE1 and p16 immunohistochemistry profiles of PXA, giant-cell glioblastoma (gcGBM) and ganglioglioma (GG).* Among PXAs, 51% of cases were both VE1-immunopositive (+) and p16-immunonegative (–). This combination was not observed among 28 giant-cell glioblastomas, which were VE1-negative in all cases and either p16-negative or p16-positive. Among gangliogliomas, combined VE1-positive and p16-negative results were observed in only 3/63 cases (5%), the majority being VE1-positive and p16-positive. Data on ganglioglioma from Koelsche *et al* (24). Magnification: 200×.

negativity and p16 loss) were accordingly not observed in giant-cell glioblastoma. Very recently, the exceedingly rare epithelioid glioblastoma has shown a high prevalence of *BRAF* V600E mutations (21). These tumors would probably have a higher occurrence of combined VE1 positivity and p16 loss. Future confirmation of this hypothesis is currently required, possibly together with a more precise definition of epithelioid glioblastoma and delineation from PXA-AF.

In ganglioglioma we observed the combined features of VE1 positivity and p16 loss in as few as 5% of cases (24). Thus, combined analyses may prove helpful in delineating PXA from giant-cell glioblastoma and ganglioglioma, especially in small-sized specimens. In clinical routine, the need may be for delineation either from ganglioglioma or from giant-cell glioblastoma, but usually not for both at the same time. Thus, in many cases, performing only the VE1 assay for the differentiation of PXA from giant-cell glioblastoma and only the p16 assay for differentiation from ganglioglioma may also be sufficient.

CONCLUSION

BRAF V600E mutations are very frequent in both PXA II and PXA-AF and nearly always present in PXAs located in the temporal lobe. *BRAF* V600E mutation is further associated with CD34 positivity and abundant formation of reticulin fibers. The combination of VE1 positivity and loss of p16 expression is seen in approximately half of PXAs but very rarely in the important differential diagnoses giant-cell glioblastoma and ganglioglioma.

ACKNOWLEDGMENTS

We thank Tanja Göck and Katja Böhmer for excellent technical assistance.

REFERENCES

1. Adeleye AO, Okolo CA, Akang EE, Adesina AM (2012) Cerebral pleomorphic xanthoastrocytoma associated with NF1: an updated review with a rare atypical case from Africa. *Neurosurg Rev* **35**:313–319, discussion 9.
2. Bettegowda C, Agrawal N, Jiao Y, Wang Y, Wood LD, Rodriguez FJ *et al* (2013) Exomic sequencing of four rare central nervous system tumor types. *Oncotarget* **4**:572–583.
3. Blumcke I, Giencke K, Wardelmann E, Beyenburg S, Kral T, Sarioglu N *et al* (1999) The CD34 epitope is expressed in neoplastic and malformative lesions associated with chronic, focal epilepsies. *Acta Neuropathol* **97**:481–490.

4. Blumcke I, Lobach M, Wolf HK, Wiestler OD (1999) Evidence for developmental precursor lesions in epilepsy-associated glioneuronal tumors. *Microsc Res Tech* **46**:53–58.
5. Bosmuller H, Fischer A, Pham DL, Fehm T, Capper D, von Deimling A *et al* (2013) Detection of the *BRAF* V600E mutation in serous ovarian tumors: a comparative analysis of immunohistochemistry with a mutation-specific monoclonal antibody and allele-specific PCR. *Hum Pathol* **44**:329–335.
6. Capper D, Weissert S, Balss J, Habel A, Meyer J, Jager D *et al* (2010) Characterization of R132H mutation-specific IDH1 antibody binding in brain tumors. *Brain Pathol* **20**:245–254.
7. Chamberlain MC (2013) Salvage therapy with *BRAF* inhibitors for recurrent pleomorphic xanthoastrocytoma: a retrospective case series. *J Neurooncol* **114**:237–240.
8. Chappe C, Padovani L, Scavarda D, Forest F, Nanni-Metellus I, Loundou A *et al* (2013) Dysembryoplastic neuroepithelial tumors share with pleomorphic xanthoastrocytomas and gangliogliomas *BRAF*(V600E) mutation and expression. *Brain Pathol* **23**:574–583.
9. Colomba E, Helias-Rodzewicz Z, Von Deimling A, Marin C, Terrones N, Pechaud D *et al* (2013) Detection of *BRAF* p.V600E mutations in melanomas: comparison of four methods argues for sequential use of immunohistochemistry and pyrosequencing. *J Mol Diagn* **15**:94–100.
10. Dahiya S, Haydon DH, Alvarado D, Gurnett CA, Gutmann DH, Leonard JR (2013) *BRAF*(V600E) mutation is a negative prognosticator in pediatric ganglioglioma. *Acta Neuropathol* **125**:901–910.
11. Deb P, Sharma MC, Tripathi M, Sarat Chandra P, Gupta A, Sarkar C (2006) Expression of CD34 as a novel marker for glioneuronal lesions associated with chronic intractable epilepsy. *Neuropathol Appl Neurobiol* **32**:461–468.
12. Dias-Santagata D, Lam Q, Vernovsky K, Vena N, Lennerz JK, Borger DR *et al* (2011) *BRAF* V600E mutations are common in pleomorphic xanthoastrocytoma: diagnostic and therapeutic implications. *PLoS ONE* **6**:e17948.
13. Dougherty MJ, Santi M, Brose MS, Ma C, Resnick AC, Sievert AJ *et al* (2010) Activating mutations in *BRAF* characterize a spectrum of pediatric low-grade gliomas. *Neuro-Oncol* **12**:621–630.
14. Geradts J, Hruban RH, Schutte M, Kern SE, Maynard R (2000) Immunohistochemical p16INK4a analysis of archival tumors with deletion, hypermethylation, or mutation of the *CDKN2*/*MTS1* gene. A comparison of four commercial antibodies. *Appl Immunohistochem Mol Morphol* **8**:71–79.
15. Giannini C, Paulus W, Louis DN, Liberski PP (2007) Pleomorphic xanthoastrocytoma. Chapter 1. In: *WHO Classification of Tumours of the Central Nervous System*. DN Louis, H Ohgaki, OD Wiestler, WK Cavenee (eds), pp. 22–24. International Agency for Research on Cancer: Lyons, France.
16. Giannini C, Scheithauer BW, Burger PC, Brat DJ, Wollan PC, Lach B, O'Neill BP (1999) Pleomorphic xanthoastrocytoma: what do we really know about it? *Cancer* **85**:2033–2045.
17. Giannini C, Scheithauer BW, Lopes MB, Hirose T, Kros JM, VandenBerg SR (2002) Immunophenotype of pleomorphic xanthoastrocytoma. *Am J Surg Pathol* **26**:479–485.
18. Hirose T, Ishizawa K, Sugiyama K, Kageji T, Ueki K, Kannuki S (2008) Pleomorphic xanthoastrocytoma: a comparative pathological study between conventional and anaplastic types. *Histopathology* **52**:183–193.
19. Ida CM, Vrana JA, Rodriguez FJ, Jentoft ME, Caron AA, Jenkins SM, Giannini C (2013) Immunohistochemistry is highly sensitive and specific for detection of *BRAF* V600E mutation in pleomorphic xanthoastrocytoma. *Acta Neuropathologica Communications* **1**:20. doi: 10.1186/2051-5960-1-20
20. Kepes JJ, Rubinstein LJ, Eng LF (1979) Pleomorphic xanthoastrocytoma: a distinctive meningocerebral glioma of young subjects with relatively favorable prognosis. A study of 12 cases. *Cancer* **44**:1839–1852.
21. Kleinschmidt-DeMasters BK, Aisner DL, Birks DK, Foreman NK (2013) Epithelioid GBMs show a high percentage of *BRAF* V600E mutation. *Am J Surg Pathol* **37**:685–698.
22. Knauf JA, Sartor MA, Medvedovic M, Lundsmith E, Ryder M, Salzano M *et al* (2011) Progression of *BRAF*-induced thyroid cancer is associated with epithelial–mesenchymal transition requiring concomitant MAP kinase and TGFβ signaling. *Oncogene* **30**:3153–3162.
23. Koelsche C, Sahm F, Paulus W, Mittelbronn M, Giangaspero F, Antonelli M *et al* (2013) *BRAF* V600E expression and distribution in desmoplastic infantile astrocytoma/ganglioglioma. *Neuropathol Appl Neurobiol* doi: 10.1111/nan.12072.
24. Koelsche C, Wohrer A, Jeibmann A, Schittenhelm J, Schindler G, Preusser M *et al* (2013) Mutant *BRAF* V600E protein in ganglioglioma is predominantly expressed by neuronal tumor cells. *Acta Neuropathol* **125**:891–900.
25. Long GV, Wilmott JS, Capper D, Preusser M, Zhang YE, Thompson JF *et al* (2013) Immunohistochemistry is highly sensitive and specific for the detection of V600E *BRAF* mutation in melanoma. *Am J Surg Pathol* **37**:61–65.
26. Okazaki T, Kageji T, Matsuzaki K, Horiguchi H, Hirose T, Watanabe H *et al* (2009) Primary anaplastic pleomorphic xanthoastrocytoma with widespread neuroaxis dissemination at diagnosis—a pediatric case report and review of the literature. *J Neurooncol* **94**:431–437.
27. Perkins SM, Mitra N, Fei W, Shinohara ET (2012) Patterns of care and outcomes of patients with pleomorphic xanthoastrocytoma: a SEER analysis. *J Neurooncol* **110**:99–104.
28. Prabowo AS, Iyer AM, Veersema TJ, Anink JJ, Schouten-van Meeteren AY, Spliet WG *et al* (2013) *BRAF* V600E mutation is associated with mTOR signalling activation in glioneuronal tumors. *Brain Pathol* **24**:52–66.
29. Purkait S, Jha P, Sharma MC, Suri V, Sharma M, Kale SS, Sarkar C (2013) *CDKN2A* deletion in pediatric versus adult glioblastomas and predictive value of p16 immunohistochemistry. *Neuropathology* **33**:405–412.
30. Reifenberger G, Kaulich K, Wiestler OD, Blumcke I (2003) Expression of the CD34 antigen in pleomorphic xanthoastrocytomas. *Acta Neuropathol* **105**:358–364.
31. Remmele W, Hildebrand U, Hienz HA, Klein PJ, Vierbuchen M, Behnken LJ *et al* (1986) Comparative histological, histochemical, immunohistochemical and biochemical studies on oestrogen receptors, lectin receptors, and Barr bodies in human breast cancer. *Virchows Arch A Pathol Anat Histopathol* **409**: 127–147.
32. Riesco-Eizaguirre G, Rodriguez I, De la Vieja A, Costamagna E, Carrasco N, Nistal M, Santisteban P (2009) The *BRAFV600E* oncogene induces transforming growth factor beta secretion leading to sodium iodide symporter repression and increased malignancy in thyroid cancer. *Cancer Res* **69**:8317–8325.
33. Schiffman JD, Hodgson JG, VandenBerg SR, Flaherty P, Polley MY, Yu M *et al* (2010) Oncogenic *BRAF* mutation with *CDKN2A* inactivation is characteristic of a subset of pediatric malignant astrocytomas. *Cancer Res* **70**:512–519.
34. Schindler G, Capper D, Meyer J, Janzarik W, Omran H, Herold-Mende C *et al* (2011) Analysis of *BRAF* V600E mutation in 1320 nervous system tumors reveals high mutation frequencies in pleomorphic xanthoastrocytoma, ganglioglioma and extra-cerebellar pilocytic astrocytoma. *Acta Neuropathol* **121**:397–405.

35. Schmidt Y, Kleinschmidt-Demasters BK, Aisner DL, Lillehei KO, Damek D (2013) Anaplastic PXA in adults: case series with clinicopathologic and molecular features. *J Neurooncol* **111**:59–69.
36. Skorokhod A, Capper D, von Deimling A, Enk A, Helmbold P (2012) Detection of *BRAF* V600E mutations in skin metastases of malignant melanoma by monoclonal antibody VE1. *J Am Acad Dermatol* **67**:488–491.
37. Sturm D, Witt H, Hovestadt V, Khuong-Quang DA, Jones DT, Konermann C *et al* (2012) Hotspot mutations in *H3F3A* and *IDH1* define distinct epigenetic and biological subgroups of glioblastoma. *Cancer Cell* **22**:425–437.
38. Sung CO, Suh YL, Hong SC (2011) CD34 and microtubule-associated protein 2 expression in dysembryoplastic neuroepithelial tumours with an emphasis on dual expression in non-specific types. *Histopathology* **59**:308–317.
39. Weber RG, Hoischen A, Ehrler M, Zipper P, Kaulich K, Blaschke B *et al* (2007) Frequent loss of chromosome 9, homozygous *CDKN2A*/p14(ARF)/*CDKN2B* deletion and low *TSC1* mRNA expression in pleomorphic xanthoastrocytomas. *Oncogene* **26**:1088–1097.
40. Zhang J, Wu G, Miller CP, Tatevossian RG, Dalton JD, Tang B *et al* (2013) Whole-genome sequencing identifies genetic alterations in pediatric low-grade gliomas. *Nat Genet* **45**:602–612.

SUPPORTING INFORMATION

Additional Supporting Information may be found in the online version of this article at the publisher's web-site.

Figure S1. VE1 overview staining (**A**) of a *BRAF* V600E-mutated pleomorphic xanthoastrocytoma (ID 59196) with weak to moderate cytoplasmic staining in the vast majority of tumor cells. Pleomorphic multinucleated giant cells presented with a strong cytoplasmic binding. The box indicates the area of higher magnification shown in (**B**). Magnification: (**A**) 25×, (**B**) 200×.

Table S1. Clinical, histological, immunohistochemical and molecular characteristics of the studied Pleomorphic Xanthoastrocytomas. ID = internal patient identifier; Loc = location; Seq = *BRAF* codon 600 sequencing; wt = wild type; V600E = substitution of valine (V) by a glutamic acid (E); 599insT = 3-bp insertion at codon position 599 resulting in an additional threonine (T); y = yes; n = no; + = positive; − = negative; VE1 = *BRAF* V600E mutation-specific antibody clone VE1; Diag = diagnosis; PXA II = pleomorphic xanthoastrocytoma, WHO grade II; PXA waf = pleomorphic xanthoastrocytoma with anaplastic features; reti = reticulin deposits; EGB = eosinophilic granular bodies; PC/MC = pleomorphic cells/multinucleated cells; XC = xanthomatous cells; TM = tumor matrix; Ro = Rosenthal fibers; Ca = calcium deposits; Hm = hemosiderin; Mi = mitoses; DN = dysplastic neurons; LC = lymphocytic cuffs; PCN = prominent capillary network; EP = endothelial proliferation; Nec = necrosis; GC = giant cells; NI = nuclear inclusions; AG = angiocentric growth; IRS = semiquantitative immunoreactive score; NA = information/data not available.

Table S2. Clinical, histological, immunohistochemical and molecular characteristics of the studied Giant Cell Glioblastomas. ID = internal patient identifier; Loc = location; Seq = *BRAF* codon 600 sequencing; wt = wild type; y = yes; n = no; + = positive; − = negative; VE1 = *BRAF* V600E mutation-specific antibody clone VE1; Diag = diagnosis; gcGBM = giant-cell glioblastoma, WHO grade IV; Reti = reticulin.

Table S3. p16, VE1 and CD34 staining status (+ = positive; − = negative) according to temporal/nontemporal location in pleomorphic xanthoastrocytoma (**A**), giant-cell glioblastoma (**B**) and ganglioglioma (**C**).